21st Australasian Fluid Mechanics Conference
Adelaide, Australia
10-13 December 2018

The effect of streamwise pressure distribution on the aeroelastic deformation of hypersonic trailing-edge flaps

S. Bhattrai, A. J. Neely, G. M. D. Currao and L. P. McQuellin

School of Engineering and Information Technology
UNSW Canberra, Australian Capital Territory, Australia

Abstract

This research studies the effects of surface pressure distribution and pressure gradient, introduced by the convex surface curvature, on the aeroelastic characteristics of hypersonic aerodynamic surfaces. An inclined trailing-edge flap model cantilevered at the back of a rigid plate is used to form a compression corner configuration. The aeroelastically-deformed convex shape of a planar flap model is taken as a baseline profile and the inclination is changed to obtain different net pressure distributions over the flap compression surface. The higher initial incidence angle of a convex surface leads to a higher pressure gradient near the flap leading-edge and a forward shift in the center of pressure. This study investigates the effects of this surface pressure distribution on the steady-state aeroelastic characteristics of the trailing-edge flap model. The numerical study was performed using the US3D code to generate laminar and turbulent solutions. The computed surface pressure distributions were used to calculate the static deformed shape of the flap. The laminar flow cases showed little difference in deformation of the flap due to a large separated region at the compression corner that resulted in identical pressure distribution regardless of the surface curvature. For the turbulent flow cases, the large pressure gradients near the compression corner changed the aeroelastic deformation of the flap with the introduction of surface curvature. For the same amount of loading, the tip deflection of a convex flap was reduced by approximately 11% in comparison to a planar flap.

Introduction

The complex aeroelastic interaction on aerodynamic surfaces of a hypersonic flight vehicle can result in significant changes in their aerodynamic characteristics. The aeroelastic response of the aerodynamic surfaces depends on the pressure distribution over the surface, or the equivalent position of the center of pressure (Cp), and the viscous effects. The surface curvature has a strong effect on the pressure distribution—primarily as a result of the inviscid compression and expansion processes. However, it also has a further effect on the boundary layer properties along the surface. If the surface is aeroelastic, this combined effect of inviscid and viscous interactions strongly determines the surface deformation, which is the subject of this study. In particular, the effect of pressure distribution over convex surfaces on the static aeroelastic deformation is studied, using both laminar and turbulent simulations. [5, 7]

Primarily, a convex wedge surface (an inclined surface turning away from the flow) introduces a flow expansion in the inviscid flow-field. Similar effects on pressure distribution can be obtained by a plate that is deformed under the action of the flow. Such aeroelastic flat plates have been studied under the HyFoil-I and HyFoil-II projects. The experiments showed that the deflected flat-plate shapes approach the profile predicted by low-fidelity modeling, e.g piston theory. [4]

The pressure and shear forces acting on the surface vary transiently during the oscillations—a phenomena that has a range of practical implications. In addition, there are critical viscous effects over the surface that significantly influence its aeroelastic response. Therefore, in addition to the inviscid flow-field effects, the expansion over the convex surface can affect the boundary layer properties as a result of the streamwise pressure gradient. Secondarily, the surface curvature effects can also be studied in context of an inclined surface as a trailing-edge device, creating a hypersonic corner-flow problem.

Such a problem has also been studied at UNSW Canberra as part of the Hypersonic Aeroelastic Control Experiment - *HyACE* project, which is investigating the methods for control of rigid and compliant hypersonic trailing-edge configurations in hypersonic ground test facilities. The HyACE models consists of actuated and non-actuated versions of rigid (thick flap) and compliant (thin flap) trailing-edge control surfaces, sharing a common planar body. [1]

Thus the effect that curvature-induced surface pressure distribution can then have on static aeroelastic deformation is a key research question of this study. This is also a practical research problem as hypersonic vehicle surfaces can have predefined curvatures, e.g. for nozzle and lifting surfaces.

The nature of this study is analytical, numerical and experimental, although only the analytical and numerical solutions are discussed here. Low-fidelity modeling using finite-element modeling (FEM) of cantilever plates (flaps) is used to obtain its deformation state, which is then taken as a reference to obtain more curved profiles of the plate. The FEM solution utilizes pressure distribution data obtained from the CFD solutions.

The deformed shape of the plate is fed back into the CFD solver in a loose 2-way fashion, as there is only one exchange between fluid and structure solvers. The structural solver is used to obtain the deformed states of the cantilever plates (flaps), which is then taken as a reference to obtain more curved profiles of the plate.

The model shown in Figure 1, consists of a 1 mm thick compliant flap with 75 mm chord. It is rigidly attached to a base plate of 12 mm thickness and 120 mm length, with a 20° wedge at the leading-edge. The baseline flap angle (θ) is 20°. The model is considered to have a span of 100 mm, for the purpose of quantifying net forces acting on it, although the numerical simulations are only carried-out in two-dimensional domains.

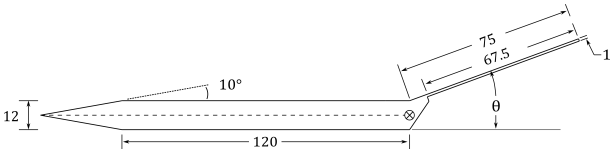

Figure 1: Elevation of the model showing relevant dimensions.

Based on the position of the cantilever support, the actual deformable length of the flap is 67.5 mm.

Analysis Methods

One-way Aeroelasticity Method

The one-way analysis is performed by coupling the fluid solver and the structural solver. The steady-state numerical simulation of the compressible flow is carried out in US3D [3]. The deformed shape of the flap is calculated using the Euler-Bernoulli beam model using the pressure distribution calculated with the fluid solver [6]. The structural solver uses steady-state CFD pressure data and nodal locations over the top and bottom of the deformable length of the plate. The test flow conditions of Mach 5.85, 75 K temperature and 755 Pa pressure correspond to the freestream conditions at the hypersonic tunnel at the University of Southern Queensland (TUSQ) [2], where the future follow-up experiments will be carried out. [1]

A two-dimensional laminar flow-field of the baseline model, with a planar flap, under the current flow conditions is shown in Figure 2. The surface pressure distribution and static deformed state of the flap is shown in Figure 3. The net pressure distribution is computed as the difference between the top and bottom surface pressures of the flap. The initial and deformed states of the flap are rotated to a horizontal orientation, such that the deformation of the flap is shown with respect to an initial cantilevered plate. The grey circular marker over the undeformed flap is the location of its original Cp. Figure 3 shows that the pressure rise is relatively gradual (with a low pressure gradient towards the compression corner), and the pressure plateaus fairly late—at a distance of around $2/3^{rd}$ of the flap chord length.

There is a loss of the net pressure force acting on the compliant flap due to its deformation. In the following section, the curved profiles with higher effective incidence angles are used to recover the net pressure forces acting on the flap. The trailing-edge deflections are compared for planar and curved flaps with similar pressure forces acting on them.

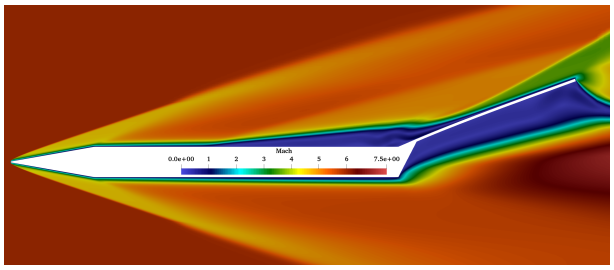

Figure 2: Mach number flow-field of the current model obtained from two-dimensional laminar simulation.

Generation of Curved Profiles

In order to generate curved flap profiles, a simple method to use the static deformed profile as the baseline curved profile was adopted. The baseline profile inclination angle at the compression corner is the same as the planar flap angle. The profile is rotated anti-clockwise by incremental angles (e.g. 2.65° and 3.31° increments used in the following discussions) such that a higher inclination angle at the compression corner is obtained.

The incremental angles are fractions of the difference between the slopes at the leading-edge and trailing-edge of the baseline curved profile. An example of this method is shown in Figure 4, where the deformed profile obtained from the one-way aeroelastic analysis of the 20° flap is taken as the baseline profile, and rotated by 2.65° in the anti-clockwise direction. The resulting leading-edge inclination angle of the flap (α_{LE}), at the

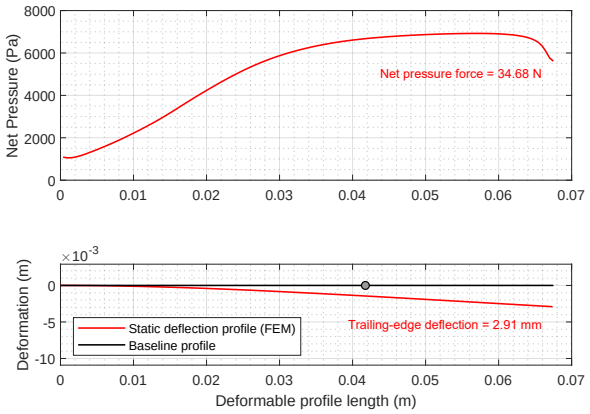

Figure 3: Pressure distribution and static deformation profile.

compression corner, is thus 22.65°. The incremental angle can be chosen to obtain curved profiles with different inclinations and net pressure distributions on the flap.

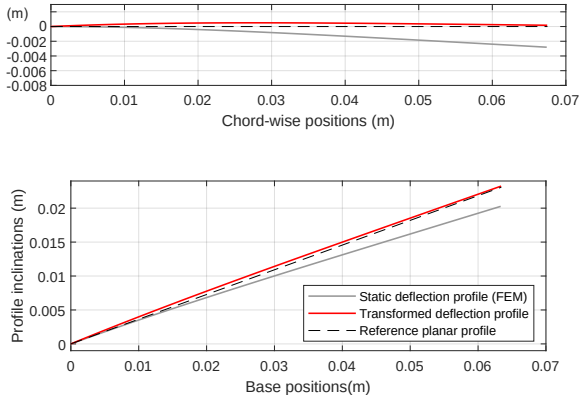

Figure 4: Convex profile obtained through an anticlockwise angular transformation of the baseline profile, plotted with respect to the horizontal (top) and the inclined planar profile (bottom).

Results and Discussion

The laminar flow-field in Figure 2 has a large separation region at the compression corner between the base plate and the flap. Since this separation region has a lower pressure than the post-reattachment region, the larger pressure values are concentrated aft of the boundary layer reattachment point. For a convex flap, the higher incidence angle of the flap near the compression corner lies in the shadow of the separation region.

This effect of the separation region on the pressure distribution is shown in Figure 5, where the net pressure distribution for a convex flap surface of $\alpha_{LE} = 23.31°$ is compared against that for the 20.0° planar flap. The laminar flow-field for the flap model is shown in Figure 6, with the large separation region extending downstream of the compression corner. It is seen in Figure 5 that the expected rise in pressure on the flap, with a higher incidence angle at the compression corner, is not achieved as a result of the shadowing effect of the boundary layer separation.

The result of this shadowing effect on the convex compliant aeroelastic deformation is that the difference between the deformation profiles for planar and convex flaps is not as significant as expected for the case in Figure 5. This is despite the fact that the integrated pressure force acting on the convex flap (=34.70 N) is close to the planar flap case in Figure 3 (=34.68

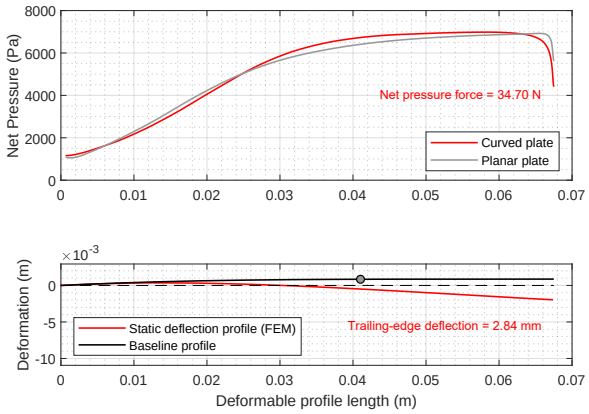

Figure 5: Laminar flow pressure distribution and static deformation profile for a convex profile with $\alpha_{LE} = 23.31°$.

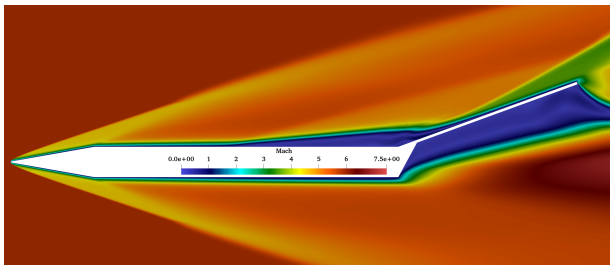

Figure 6: Mach number flow-field of the current model obtained from two-dimensional laminar simulation for the convex flap with $\alpha_{LE} = 23.31°$.

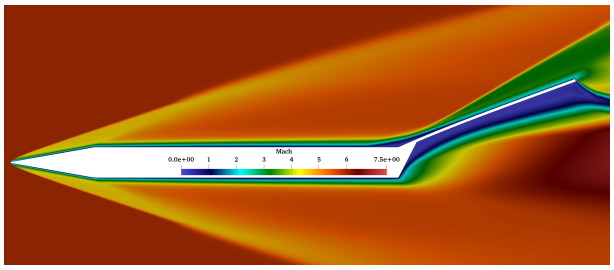

Figure 7: Mach number flow-field of the 20.0° planar flap obtained from two-dimensional turbulent simulation.

N). This is in addition to the slight forward movement of the Cp, from 41.8 mm to 41.0 mm. Therefore, in the laminar flow case of the convex flap, neither the higher inclination angles nor the measurable movement of the Cp was effectively seen in the net pressure distribution. As a result, the tip-deflection of the convex flap with $\alpha_{LE} = 23.31°$ is close to the planar 20.0° flap.

On the other hand, for a turbulent case the boundary layer separation region at the compression corner is significantly smaller than that for a laminar case—as seen in Figure 7. As a result, the oblique shock wave is attached close to the compression corner. The pressure distribution and static deformation profile for this case is shown in Figure 8. There is a sharp increase in pressure over the flap, and it reaches a plateau within a distance of $1/3^{rd}$ of the flap chord length. Therefore, there is a large pressure gradient close to the compression corner, in absence of the shadowing effect of the separation region as in the laminar case. Until there is a large fully-separated region at the compression corner, the center of pressure of the convex flap moves further upstream on a convex flap of higher incidence angle.

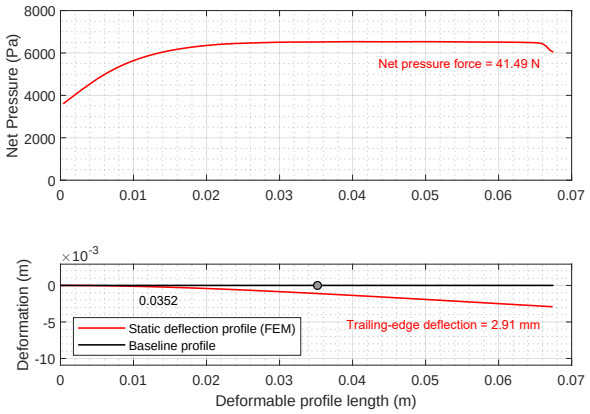

Figure 8: Turbulent flow pressure distribution and static deformation profile for a planar flap.

The results for the convex flap with $\alpha_{LE} = 23.31°$ was computed under turbulent flow conditions, and the obtained pressure distribution and deformation profiles are presented in Figure 9. There is a significant increase in pressure (with a larger pressure gradient)—an expected result of the higher initial angles of the convex surface—that approaches the pressure distribution for the planar flap. The net pressure force acting on the convex flap is 43.57 N, greater than for the planar case (=41.49 N), while the Cp of the convex flap has shifted from the planar position of 35.2 mm to an upstream location of 33.2 mm. The result of these changes is directly seen in the static aeroelastic deformation of the convex flap, where the tip deflection is slightly lower than the planar case despite a higher pressure load acting on it.

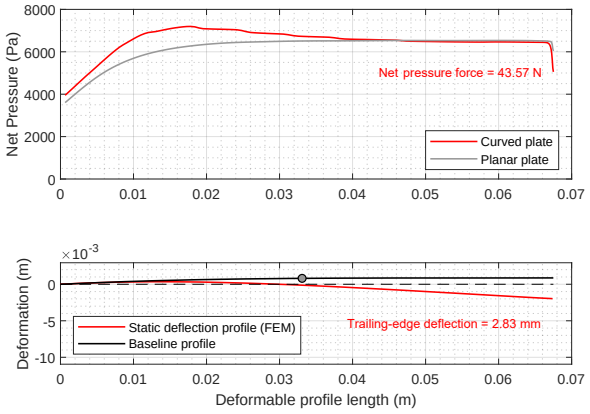

Figure 9: Turbulent flow pressure distribution and static deformation profile for a convex profile with $\alpha_{LE} = 23.31°$.

To observe a more direct effect of the convex curvature on the flap deformation, a case that has approximately the same net pressure force acting on it as for the planar flap case in Figure 8 was obtained and analysed. The pressure distribution and static deformation profiles are shown in Figure 10. This convex profile has an α_{LE} of 22.65° and the net pressure force acting on it is 41.57 N—close to the 41.49 N force acting on the planar case. The location of Cp is at 33.2 mm, forward of the planar Cp location. The resulting flap tip deflection is 2.57 mm, which is around 11% less than for the planar case.

In Table 1, the trailing-edge deflection values for each of the above cases are compared with respect to the net pressure forces acting on the flaps and the Cp locations. As previously discussed, in a laminar flow, the pressure distribution over the con-

Laminar flow simulation			
Flap case	Net pressure force	Cp location	Flap tip deflection
Planar	34.68 N	41.8 mm	2.91 mm
Convex (α_{LE} = 23.31°)	34.70 N	41.0 mm	2.84 mm
Turbulent flow simulation			
Flap case	Net pressure force	Cp location	Flap tip deflection
Planar	41.49 N	35.2 mm	2.91 mm
Convex (α_{LE} = 22.65°)	41.57 N	33.2 mm	2.57 mm
Convex (α_{LE} = 23.31°)	43.57 N	33.2 mm	2.83 mm

Table 1: Comparison of net pressure load, Cp location and trailing-edge deflection for planar and curved profiles.

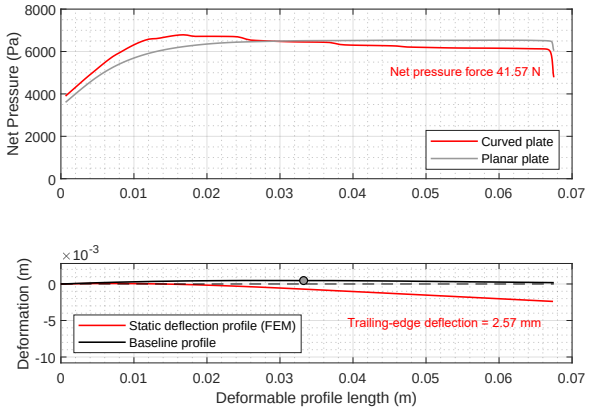

Figure 10: Turbulent flow pressure distribution and static deformation profile for a convex profile with an initial inclination of 22.65°.

vex flap does not get significantly affected by the higher α_{LE}, due to the shadowing effect of the large boundary layer separation region at the compression corner. Therefore, the forward shift of the Cp is small, and the flap tip deflection is reduced by less than 2.5% of the corresponding planar flap case despite equivalent net pressure forces acting on both the flaps. On the other hand, in a turbulent flow the boundary layer separation is much reduced in size, and the forward shift of the Cp and reduction of flap tip deflection are relatively more significant. Initial tests conducted at TUSQ with the current HyACE model have shown the boundary layer to be laminar at the compression corner. Therefore, the current study shows that the configuration may not be suitable for studying the curvature-induced pressure distribution and its effect on compliant aerodynamic surfaces.

Conclusions

Surface pressure distributions with forward locations of Cp can be created with a cambered surface profile, which can lead to a better control of aeroelastic deformation. Such techniques can be used to study hypersonic aerodynamic control surfaces with better control authority by reducing aeroelastic deformation, and the use of thinner aerodynamic surfaces. The effects of surface curvature on the aeroelastic deformation of compliant flap was presented in this paper, and the main findings of the analyses can be summarized as follows:

1. The effect of curvature was on the streamwise pressure distribution over a trailing-edge flap, which accompanied a forward shift in location of the Cp when a pressure gradient near the flap leading edge was higher.

2. In turbulent flow cases the higher pressure gradient was achieved near the compression corner. In laminar flows, the large boundary layer separation region at the corner shadows the curvature effect. As a result, a significant difference in aeroelastic deformation was not observed for the laminar cases.

3. An approximately 11% percent reduction in trailing-edge deflection from a planar flap case was observed for a convex flap in turbulent flow cases, under similar pressure forces.

4. While the current study only considers convex flaps with a constant camber, further reduction in the aeroelastic deformation may be possible with the introduction of additional curvature to the flap profile. From the flow-field comparison, in the presence of small curvatures the boundary layer separation region does not change significantly.

Acknowledgements

This research was supported by the USAF AFOSR Grant No. FA2386-16-1-4024. This research was undertaken with the assistance of resources and services from the National Computational Infrastructure (NCI), which is supported by the Australian Government.

References

[1] Bhattrai S., McQuellin L.P., Currao G.M., Neely A.J., and Buttsworth D.R., Influence of hypersonic fluid-structure interaction on the control authority of a trailing-edge flap, *22nd AIAA International Space Planes and Hypersonics Systems and Technologies Conference*, 2018, 5265.

[2] Buttsworth D.R., Ludwieg Tunnel Facility with Free Piston Compression Heating for Supersonic and Hypersonic Testing, *Proceedings of the 9th Australian Space Science Conference, National Space Society of Australia Ltd.*, 2010, 153–162.

[3] Candler G. V. Candler, Johnson H.B., Nompelis I., Gidzak V.M., Subbareddy P.K. and Bernhardt M., Development of the US3D Code for Advanced Compressible and Reacting Flow Simulations, *AIAA Paper*, **1893**, 2015.

[4] Currao G., Neely A., Buttsworth D.R. and Choudhary R., Measurement and Simulation of Hypersonic Fluid-Structural Interaction on a Cantilevered Plate in a Mach 6 Flow, *15th Dynamics Specialists Conference, American Institute of Aeronautics and Astronautics*, 2016.

[5] Mohammadian S., Viscous Interaction over Concave and Convex Surfaces at Hypersonic Speeds, *J. Fluid Mech.*, **55(1)**, 1972, 163-175.

[6] Reddy J.N., An Introduction to the Finite Element Method, *Asia Higher Education Engineering/Computer Science Mechanical Engineering*, McGraw-Hill, 2006.

[7] Wang Q.C., and Wang Z.G and Zhao Y.X, The Impact of Streamwise Convex Curvature on the Supersonic Turbulent Boundary Layer, *Phy. Fluids*, **29(9)**, 2017, 116106.